

Tight focusing of plane waves from micro-fabricated spherical mirrors

J. Goldwin and E. A. Hinds

*Centre for Cold Matter,
Department of Physics, Division of Quantum Optics and Laser Science,
Imperial College, London SW7 2AZ, United Kingdom*

j.goldwin@imperial.ac.uk

<http://www3.imperial.ac.uk/ccm>

Abstract: We derive a formula for the light field of a monochromatic plane wave that is truncated and reflected by a spherical mirror. Within the scalar field approximation, our formula is valid even for deep mirrors, where the aperture radius approaches the radius of curvature. We apply this result to micro-fabricated mirrors whose size scales are in the range of tens to hundreds of wavelengths, and show that sub-wavelength focusing (full-width at half-maximum intensity) can be achieved. This opens up the possibility of scalable arrays of tightly focused optical dipole traps without the need for high-performance optical systems.

© 2022 Optical Society of America

OCIS codes: (130.3990) Micro-optical devices; (260.1960) Diffraction theory; (020.7010) Laser trapping.

References and links

1. N. Schlosser, G. Reymond, I. Protsenko, and P. Grangier, "Sub-poissonian loading of single atoms in a microscopic dipole trap," *Nature (London)* **411**, 1024-1027 (2001).
2. N. Schlosser, G. Reymond, and P. Grangier, "Collisional Blockade in Microscopic Optical Dipole Traps," *Phys. Rev. Lett.* **89**, 023005 (2002).
3. Y. R. P. Sortais, H. Marion, C. Tuchendler, A. M. Lance, M. Lamare, P. Fournet, C. Armellin, R. Mercier, G. Messin, A. Browaeys, and P. Grangier, "Diffraction-limited optics for single-atom manipulation," *Phys. Rev. A* **75**, 013406 (2007).
4. B. Darquié, M. P. A. Jones, J. Dingjan, J. Beugnon, S. Bergamini, Y. Sortais, G. Messin, A. Browaeys, P. Grangier, "Controlled Single-Photon Emission from a Single Trapped Two-Level Atom," *Science* **309**, 454-456 (2005).
5. M. Weber, J. Volz, K. Saucke, C. Kurtsiefer, and H. Weinfurter, "Analysis of a single-atom dipole trap," *Phys. Rev. A* **73**, 043406 (2006).
6. M. K. Tey, Z. Chen, S. A. Aljunid, B. Chng, F. Huber, G. Maslennikov, C. Kurtsiefer, "Strong interaction between light and a single trapped atom without a cavity," arXiv:0802.3005v3 (2008), <http://uk.arxiv.org/abs/0802.3005v3>.
7. B. Lounis and M. Orrit, "Single-photon sources," *Rep. Prog. Phys.* **68**, 1129-1179 (2005).
8. E. Waks, C. Santori, and Y. Yamamoto, "Security aspects of quantum key distribution with sub-Poisson light," *Phys. Rev. A* **66**, 042315 (2002).
9. E. Knill, R. Laflamme, and G. J. Milburn, "A scheme for efficient quantum computation with linear optics," *Nature (London)* **409**, 46-52 (2001).
10. M. Oxborrow and A. G. Sinclair, "Single-photon sources," *Contemp. Phys.* **46**, 173-206 (2005).
11. M. Sondermann, R. Maiwald, H. Koneermann, N. Lindlein, U. Peschel, and G. Leuchs, "Design of a mode converter for efficient light-atom coupling in free space," *Appl. Phys. B* **89**, 489-482 (2007).
12. S. J. van Enk and H. J. Kimble, "Strongly focused light beams interacting with single atoms in free space," *Phys. Rev. A* **63**, 023809 (2001).
13. M. K. Tey, S. A. Aljunid, F. Huber, B. Chng, Z. Chen, G. Maslennikov, and C. Kurtsiefer, "Interfacing light and single atoms with a lens," arXiv:0804.4861v2 (2008), <http://uk.arxiv.org/abs/0804.4861v2>.

14. S. Eriksson, M. Trupke, H. F. Powell, D. Sahagun, C. D. J. Sinclair, E. A. Curtis, B. E. Sauer, E. A. Hinds, Z. Muktadir, C. O. Gollasch and M. Kraft, "Integrated optical components on atom chips," *Eur. Phys. J. D* **35**, 135-139 (2005).
 15. M. Trupke, E. A. Hinds, S. Eriksson, E. A. Curtis, Z. Muktadir, E. Kukharenska, and M. Kraft, "Microfabricated high-finesse optical cavity with open access and small volume," *Appl. Phys. Lett.* **87**, 211106 (2005).
 16. For a recent review of atom chip experiments, see J. Fortágh and C. Zimmermann, "Magnetic microtraps for ultracold atoms," *Rev. Mod. Phys.* **79**, 235 (2007).
 17. M. Born and E. Wolf, *Principles of Optics*, 7th edition, (Cambridge University Press, Cambridge, 1999).
 18. The software used in this work is available from <http://ab-initio.mit.edu/wiki/index.php/Meep>.
 19. A. Taflov and S. C. Hagness, *Computational Electrodynamics: The Finite-Difference Time-Domain Method*, (Artech, Norwood, MA, 2000).
 20. A. Farjadpour, D. Roundy, A. Rodriguez, M. Ibanescu, P. Bermel, J. D. Joannopoulos, S. G. Johnson, and G. Burr, "Improving accuracy by subpixel smoothing in the finite-difference time domain," *Opt. Lett.* **31**, 2972-2974 (2006).
 21. M. Lax, W. H. Louisell, and W. B. McKnight, "From Maxwell to paraxial wave optics," *Phys. Rev. A* **11**, 1365-1370 (1975).
 22. G. P. Agrawal and M. Lax, "Free-space wave propagation beyond the paraxial approximation," *Phys. Rev. A* **27**, 1693-1695 (1983).
-

1. Introduction

Spherical mirrors are widely used, for example in the telescope, to collect light from a distant object and focus it to a point. In practice this produces not a point but a distribution of light over a finite region in the vicinity of the focus. Analysis of this behavior involves two classic topics in optics — diffraction from a circular aperture and spherical aberrations of the mirror. Typically, the spot size is characterized by a figure of merit such as transverse aberration or root-mean-squared blur radius. However, in a variety of modern applications, such as data storage, optical tweezers or atom trapping, it is only important to have a narrow central spot even though this may be accompanied by a broad distribution of low intensity in the wings. For such applications, the analysis requires a new approach, which we develop here.

Our own interest is in making an array of atom traps so small that each trap can hold one atom (or none), but not two. If a second atom is caught, the two interact through a light-induced, inelastic collision and both are kicked out of the trap — an effect known as collisional blockade [1, 2]. The ejection of atom pairs occurs promptly provided the spot size of the trapping light is below $\sim 1\mu\text{m}$ [3], which is roughly the size of the optical wavelength λ . One important application for such traps is the production of single photons on demand [4, 5, 6], which can then be used as a powerful resource for quantum cryptography and quantum information processing [7, 8, 9, 10].

There is a growing literature concerned with strong focusing of light onto single atoms in free space, as a means of achieving efficient atom-light coupling. A scheme proposed in Ref. [11] aims to emulate the field radiated from a single atom. This ideal can be approached using a parabolic reflector to focus light with highly sculpted intensity and phase profiles, but the scheme does not seem suitable for scaling to large arrays of traps. In Ref. [12], van Enk and Kimble considered the simpler case of focusing a uniformly polarized Gaussian beam with a lens that imposes a Gaussian phase profile. They were able to achieve a three-dimensional solution for the light field in the region of the focal point. Tey *et al.* recently extended this analysis to the case of a spherically converging Gaussian wave [13], which gave somewhat better coupling. Both of these calculations neglect the aberrations produced by a real imaging system.

In the work presented here, we consider focusing by spherical mirrors and we treat the aberrations of the mirror exactly. No high-performance optical system is required and the method offers a simple way to achieve large arrays of traps that are tight enough to produce a strong collisional blockade for alkali atoms. The idea is to use arrays of hemispherical mirrors, typ-

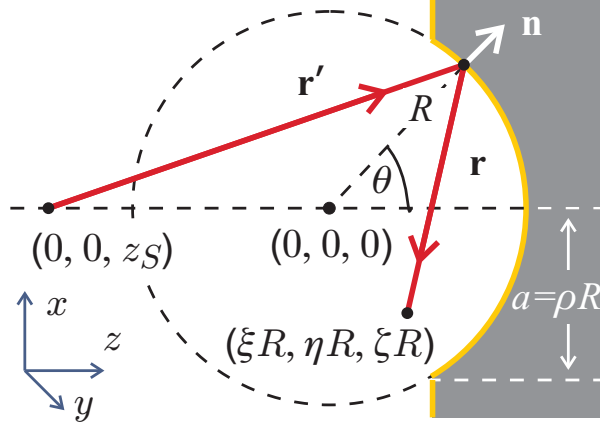


Fig. 1. (Color online) Light incident along the path \mathbf{r}' is reflected at a point on the spherical mirror surface, then propagates along \mathbf{r} to the point of observation (cartesian coordinates $(\xi R, \eta R, \zeta R)$).

ically with radius of curvature $R \sim 100 \mu\text{m}$, that are lithographically etched directly into the surface of a silicon wafer [14, 15] and covered with a reflective coating. An incoming plane wave may then be focused to an array of points in a plane near the surface of the wafer, to produce a tight optical trap above each reflector. Once integrated into an atom chip [16], these traps may be loaded either directly from a surface magneto-optical trap, or from a magnetic guide with optical molasses added to enable the blockade.

In calculating the characteristics of these microtraps, we found it necessary to consider both the diffraction and the spherical aberrations. This led us to derive an analytical expression for the distribution of the light near the optic axis of a spherical mirror, which is applicable for wide-angle reflectors and does not seem to have appeared previously in the literature. Although the full problem can be solved numerically with a high-performance computer and sufficient patience, our formula has the advantage that it can be evaluated more or less instantaneously. In the rest of this paper, we derive our analytical results, compare them with full numerical simulations, and show that the silicon micro-mirrors are indeed suitable for making sub-wavelength atom traps.

2. Theory

Figure 1 shows a schematic micro-mirror with radius of curvature R centered on the point $(0, 0, 0)$, illuminated by a point source at position $(0, 0, z_S)$. We take $z_S \rightarrow -\infty$, so that the incident light is collimated and parallel to the optic axis. If the light were incident on a simple circular hole of radius a , the amplitude of the output in the far field propagating at angle α to the optic axis would be given by $J_1(ka \sin \alpha) / \sin \alpha$, where k is the wavenumber $2\pi/\lambda$ and J_1 is the Bessel function [17]. As a starting point, let us consider ideal imaging that satisfies the Abbe sine criterion and focuses incident collimated light onto the plane $z = R/2$. In the image plane, the rays incident at angle α have an off-axis displacement of $(R/2) \tan \alpha$. The resulting Fraunhofer diffraction pattern in the focal plane has a radius at half-maximum intensity, $r_{1/2}^{\text{diff}}$, given by

$$\frac{r_{1/2}^{\text{diff}}}{\lambda} = \frac{1.62 R/2}{2\pi a} = \frac{0.13}{\rho}, \quad \left(\rho \leq \frac{1}{2} \right). \quad (1)$$

Here, we have neglected the difference between $\sin \alpha$ and $\tan \alpha$, since we are only interested in apertures having $a \gg \lambda$, which produce small angles of diffraction. The aperture size is conveniently expressed by the dimensionless ratio $\rho \equiv a/R$. For a spherical mirror, $\rho \leq 1$, but for imaging that satisfies the Abbe criterion, the numerical aperture reaches its maximum value of 1 when the input radius is equal to the focal length (see [17], §4.5.1). Thus the maximum aperture for our ideal optic is $\rho = 1/2$, giving a minimum spot size according to Eq. (1) of 0.26λ . Throughout this paper we use the phrase ‘‘spot size’’ to mean radius at half-maximum intensity.

This result captures the essence of the diffraction but does not treat the focusing correctly since a large-aperture mirror exhibits numerous orders of aberration. We therefore adopt Kirchhoff’s diffraction theory in order to estimate the spot size more accurately. The incident light is assumed to illuminate the mirror surface uniformly. Secondary waves then radiate to the observation point $\mathbf{x}_O = (\xi R, \eta R, \zeta R)$, illustrated in Fig. 1. For simplicity we ignore the incoming beam and reflections from the flat part of the mirror because we are interested in the focal region, where the reflected intensity is relatively high. Kirchhoff’s integral for the diffracted wave $\psi_{\perp}^{(0)}$ is then

$$\psi_{\perp}^{(0)}(\mathbf{x}_O) = \frac{1}{4\pi} \iint \left[\frac{e^{ikr'}}{r'} \nabla_{\mathbf{n}} G(r) - G(r) \nabla_{\mathbf{n}} \frac{e^{ikr'}}{r'} \right] d\mathcal{A}, \quad (2)$$

where $d\mathcal{A} = R^2 d\phi d\cos \theta$ is an element of area on the curved surface of the mirror. The scalar r' is the modulus of the vector \mathbf{r}' shown in Fig. 1, and similarly for r . The free-space Green function for the light field is $G(r) = \exp(ikr)/r$, and $\nabla_{\mathbf{n}}$ denotes the gradient taken along \mathbf{n} , the normal to the mirror surface. Since the observation points of interest will be many wavelengths away from the mirror surface, we can assume that $kr \gg 1$ and therefore

$$\nabla_{\mathbf{n}} \frac{e^{ikr}}{r} \approx ik \cos(\mathbf{n}, \mathbf{r}) \frac{e^{ikr}}{r}, \quad (3)$$

where $\cos(\mathbf{n}, \mathbf{r})$ is the cosine of the angle between \mathbf{r} and \mathbf{n} . A similar expression holds for $r \rightarrow r'$.

Taking $z_S \rightarrow -\infty$, the source term $\exp(ikr')/r' \rightarrow \psi \exp(ikR \cos \theta)$, with the complex amplitude ψ being constant. Then

$$\psi_{\perp}^{(0)} = \frac{ik\psi}{4\pi} \iint \frac{e^{ik(r+R\cos\theta)}}{r} [\cos(\mathbf{n}, \mathbf{r}) - \cos(\mathbf{n}, \mathbf{r}')] d\mathcal{A}. \quad (4)$$

With this collimated input, $\cos(\mathbf{n}, \mathbf{r}')$ is just $\cos \theta$, while $\cos(\mathbf{n}, \mathbf{r})$ is given by

$$r \cos(\mathbf{n}, \mathbf{r}) = -R(1 - \xi \cos \phi \sin \theta - \zeta \cos \theta), \quad (5)$$

where we have taken $\eta = 0$ without loss of generality. Since the light is to be tightly focused near the optical axis, we need only consider observation points where $\xi \ll 1$. Expanding r to first order around $\xi = 0$, we obtain

$$\begin{aligned} \frac{r}{R} &\approx \sqrt{1 + \zeta^2 - 2\zeta \cos \theta} - \frac{\xi \sin \theta \cos \phi}{\sqrt{1 + \zeta^2 - 2\zeta \cos \theta}} \\ &\equiv \delta_0 + \xi \delta_1 \cos \phi. \end{aligned} \quad (6)$$

Returning now to Eq. (4), we eliminate the two cosines and replace r by $R\delta_0$ everywhere except in the exponent. There, we keep the $R\xi\delta_1$ term as well and integrate over ϕ , giving

$$\psi_{\perp}^{(0)} = \frac{k\psi}{4\pi i} \iint \frac{e^{i\kappa(\mu + \delta_0 + \xi \delta_1 \cos \phi)}}{R\delta_0} \left(\mu + \frac{1 - \zeta\mu}{\delta_0} \right) d\mathcal{A}$$

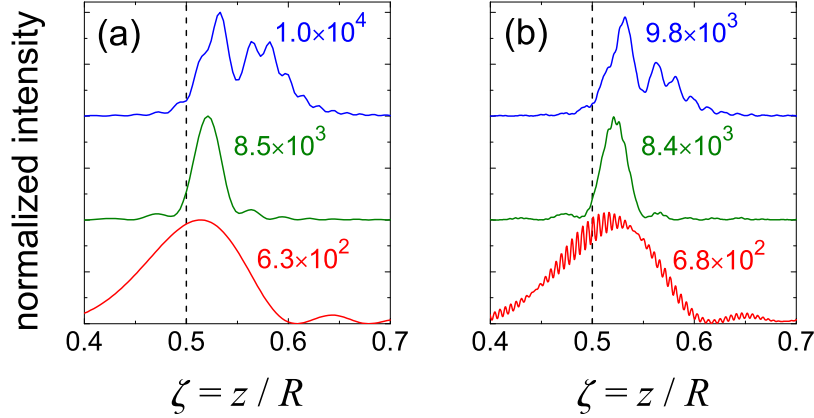


Fig. 2. (Color online) Intensity distribution on axis with $R = 100\lambda$ for values of mirror aperture $\rho = 0.2$ (bottom), 0.4 (middle), 0.6 (top). These are offset vertically for clarity. Labels give the peak intensity for unit incident intensity. (a) Prediction of Eq. (7). Curves are re-scaled to be equal in height. (b) Result of full numerical integration of Maxwell's equations. Each curve has the same scale as the corresponding curve in (a). Dashed lines mark the geometrical focus at $\zeta = 1/2$.

$$= \frac{\kappa \Psi}{2i} \int_{\mu_0}^1 \frac{e^{i\kappa(\mu+\delta_0)}}{\delta_0} \left(\mu + \frac{1-\zeta\mu}{\delta_0} \right) J_0 \left(\frac{\kappa\xi}{\delta_0} \sqrt{1-\mu^2} \right) d\mu, \quad (7)$$

where $\kappa = kR$, $\mu = \cos \theta$ and $\mu_0 = (1 - \rho^2)^{1/2}$. This is our main result.

In the limit of small mirror aperture, *i.e.* small ρ and θ , $\delta_0 \rightarrow (1 - \zeta)$, $\mu \rightarrow 1$, $(1 - \mu^2)^{1/2} \rightarrow \theta$ and $d\mu \rightarrow -\theta d\theta$. Then

$$\left| \psi_{\perp}^{(0)} \right| \rightarrow |\psi| \left(\frac{\rho q}{2} \right) \left| \frac{2J_1(q\xi)}{q\xi} \right|, \quad q = \frac{\kappa \rho}{1 - \zeta}. \quad (8)$$

Thus the radius at half-maximum intensity is

$$r_{1/2} = 0.26(1 - \zeta)\lambda/\rho \quad (\text{when } \rho \ll 1). \quad (9)$$

Evaluated in the focal plane $\zeta = 1/2$, this duplicates Eq. (1), as one would expect in this limit where the mirror becomes an ideal thin element. The position of maximum intensity lies on the z axis, but not at $\zeta = 1/2$. In this small aperture limit, the intensity increases as the mirror is approached because the spreading of the light due to diffraction dominates over the focusing due to the curvature of the mirror surface: this is the limit of small Fresnel number.

3. Results

Figure 2(a) shows the intensity on axis versus position, as given by Eq. (7) for three larger values of the aperture. These all have Fresnel numbers greater than unity and exhibit peaks close to $\zeta = 0.5$. At first, as the aperture is increased, the light becomes more concentrated axially, giving rise to a narrower peak at $\rho = 0.4$ (middle) than at $\rho = 0.2$ (bottom). With even larger aperture, however, secondary structure appears on the large- ζ side of the main peak. This is due

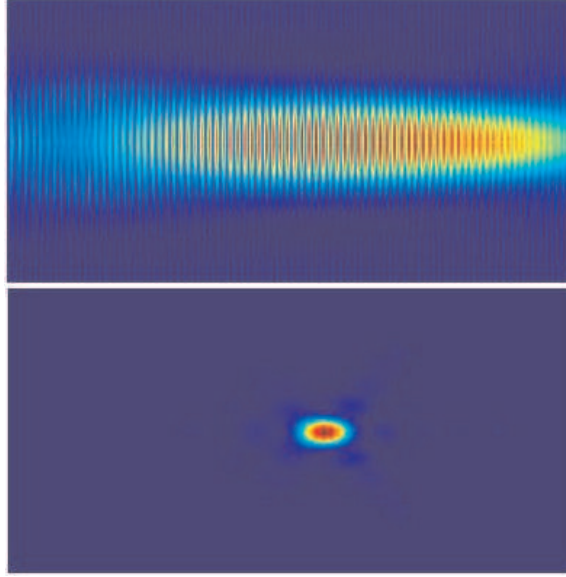


Fig. 3. (Color online) Simulated intensity distributions of light outside concave spherical mirrors with radius of curvature $R = 100\lambda$, etched in a plane substrate. The field of view is 10λ (vertical) $\times 40\lambda$ (horizontal), centered on $z = R/2$, with the mirror to the right. The calculations are done by numerical integration of Maxwell's equations. Upper image: $\rho = 0.1$. Lower image: $\rho = 0.4$.

to spherical aberration, *i.e.* to rays that are incident increasingly far from the axis and therefore cross the axis at larger values of ζ after reflection. In order to test these detailed predictions of Eq. (7), we have integrated Maxwell's equations numerically using freely available software [18], based on the finite-difference time-domain method [19], with sub-pixel smoothing for accuracy at sharp interfaces [20]. Our resolution varies from 20 to 32 pixels per wavelength and we treat the mirror surface as a perfect conductor. We exploit the cylindrical symmetry of the problem by taking the incident plane-wave beam to be circularly polarized. Figure 3 illustrates the solutions obtained in this way for $\rho = 0.1$ (upper frame) and $\rho = 0.4$ (lower frame). The numerical results for the intensity on axis are plotted in Fig. 2(b) for comparison with the plots shown in Fig. 2(a).

For the smallest aperture, there is good agreement on the shape and intensity of the curve, but the numerical integration exhibits additional rapidly oscillating fringes, similar to those seen in the upper frame of Fig. 3. These are due mainly to interference between the incident plane-wave and the field reflected from the mirror. The same effect can be captured qualitatively by adding the incident field to Eq. (7). Such an intensity distribution could be useful for making a tightly confining optical lattice but would not be chosen when a single, well-defined atom trap is required. The full numerical solution with medium aperture, shown in the lower frame of Fig. 3 and in the central curve of Fig. 2(b), agrees very well with our analytical result. The interference fringes are much less evident here, as the amplitude of the reflected wave is much higher. There is also good agreement in the case of the largest aperture, except that the subsidiary structure due to spherical aberration is slightly smaller in the exact solution. This is because the electric fields of rays coming from the outer parts of the mirror are significantly inclined and should be added as vectors, whereas Eq. (7), based on the scalar wave equation, adds them as scalars. We conclude that an aperture $\rho = 0.4$ is a good choice for achieving a single optical dipole trap

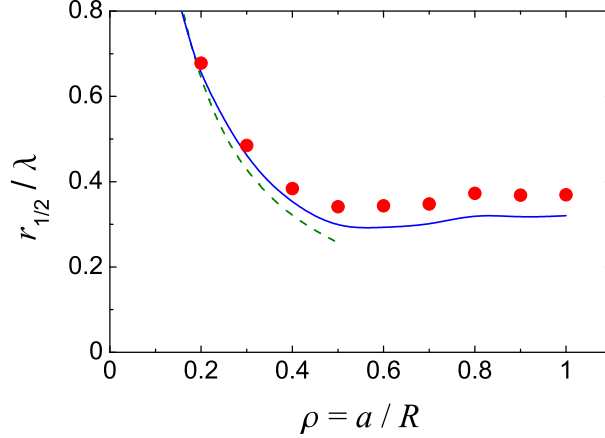


Fig. 4. (Color online) Normalized spot size $r_{1/2}/\lambda$ as a function of aperture ρ with $R = 100\lambda$. Solid line: radius given by Eq. (7) evaluated at the peak of the axial intensity distribution. Dashed line: radius given by Eq. (1) for an ideal optic with focal length $R/2$. Dots: full numerical integration of Maxwell's equations.

with tight axial confinement, and that this is well described by Eq. (7). Note that the use of a larger aperture does not add substantially to the peak intensity.

We turn now to the radial width of the intensity distribution. The dashed curve in Fig. 4 shows the ideal value $r_{1/2}^{\text{diff}}$, given by Eq. (1), plotted against the aperture ρ up to the maximum value possible, $\rho = 1/2$. This suggests that apertures $\rho > 0.2$ should produce very small spot sizes. The solid line, derived from Eq. (7), shows that although the spot size is somewhat increased by the mirror depth and the aberrations neglected in Eq. (1), it is still well below $\lambda/2$. We calculate this width not in the focal plane $\zeta = 1/2$ but at the value of ζ where the on-axis intensity is maximum, since that is where the optical dipole trap is actually formed. The dots show the widths obtained from the full numerical integration of Maxwell's equations. Near $\rho = 0.2$, these agree closely with the widths derived from Eq. (7), but as the aperture opens, we see that the full solution gives a slightly larger spot size. This broadening is another manifestation of the vector nature of the light field. We conclude that parallel light, incident on a spherical micro-mirror with aperture $\rho = 0.4$, can produce an optical dipole trap that is well described by Eq. (7), with spot size $< \lambda/2$.

Concerning the vector nature of the field, this is transverse on axis and follows the polarisation of the input light. Off axis, however, the field acquires a z -component, given in the case of small ρ by [21, 22]

$$\psi_z^{(1)}(\xi, \zeta) = \frac{i}{\kappa} \frac{\partial}{\partial \xi} \left[\psi_{\perp}^{(0)}(\xi, \zeta) \right] . \quad (10)$$

This produces the increase in $r_{1/2}$ that we have noted above. We can estimate the size of the z -component from the derivative of Eq. (8), even when the mirror is not strictly in the small ρ limit. Near the focal plane and to first order in ξ , this gives $\left| \psi_z^{(1)}/\psi_{\perp}^{(0)} \right| \simeq 2\pi\rho^2 x/\lambda$. For $\rho = 0.4$ this ratio grows from zero on axis to 0.4 at $x = r_{1/2} = 0.4\lambda$. Thus, the trapped atom will not see a constant polarization as it explores the volume of the trap, but assuming that its kinetic energy is significantly less than half the trap depth, the polarization will be approximately that

of the input light.

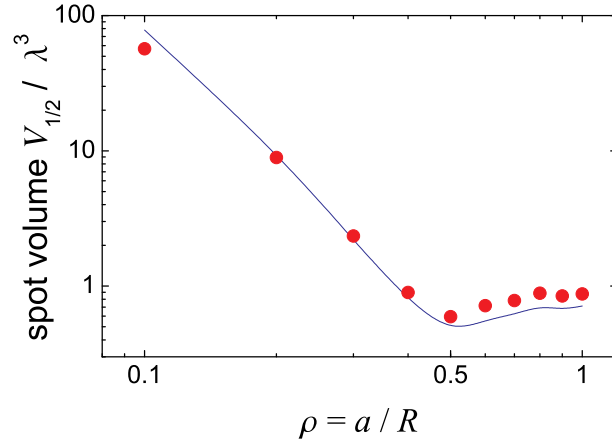


Fig. 5. (Color online) Normalized spot volume, as defined in the text, for varying aperture sizes and $R = 100\lambda$. Dots: numerical integration of Maxwell’s equations. Line: results from Eq. (7).

For collisional blockade experiments, the focal spot must have a small *volume*, in addition to small $r_{1/2}$, in order to ensure no more than a single atom per trap. We define the spot volume $V_{1/2}$ as the volume within the contour of half-maximum intensity, which is plotted in Figure 5 as a function of ρ . For small apertures, we find $V_{1/2} \propto r_{1/2}^4 / \lambda$, as expected from dimensional arguments. For larger apertures, $V_{1/2}$ drops to a minimum near $\rho = 0.5$, then rises to a level just below λ^3 . As a point of reference, the spot volume for an ideal Gaussian TEM₀₀ beam is given by $V_{1/2} = 41.8 r_{1/2}^4 / \lambda$, which is $2.6\lambda^3$ for $r_{1/2} = \lambda/2$. Once again, Eq. (7) provides a very good approximation to the exact solution. Finally we note that although all the simulations shown in this article have taken $R = 100\lambda$, this is not a critical requirement. When R is increased from 60λ to 140λ , the spot volume obtained by numerical integration for $\rho = 0.4$ grows by less than 14%, though of course the constraint on surface quality of the mirror becomes more demanding.

4. Conclusion

In conclusion we have derived a useful formula for the field distribution in front of a spherical mirror illuminated by a plane wave. Using this result we have shown that a modern micro-fabricated mirror of order $10\text{-}100\lambda$ in size can produce either a tight optical lattice, or a single spot with little additional structure, having a radius at half-maximum intensity well below $\lambda/2$. The fabrication method makes it straightforward to scale this up to a large number of spots in any desired array. This method is therefore suitable for building atom traps for applications in quantum information processing, or for any other application where tight focusing is required and the low-intensity wings of the spot are unimportant.

Acknowledgements

This work was supported by the Royal Society, by EPSRC projects “Cold Atoms in Micro-traps” and QIPIRC, and by the European Commission projects SCALA and HIP. We thank the developers of MEEP at MIT for providing the free simulation package used in this work.